Fermi National Accelerator Laboratory
Particle Physics Division

Mechanical Department Engineering Note

Number: *MD-Eng/01-001* **Date:** *31 May 2001*

Project: *BTeV Pixels*

Project Internal Reference: *N/A*

Title: ***Investigation of Two-Phase Cooling Performance for the Proposed BTeV Pixel Detector***

Author(s): *Greg Derylo*

Reviewer(s): ---

Key Words: BTeV / 2-Phase Cooling

Abstract/Summary:

The use of two-phase cooling was investigated for use with the current BTeV pixel beryllium ladder cooling channel design. Of the three refrigerants investigated, the R134a had the best pressure drop and heat transfer performance. Small pressure drops and low, relatively uniform wall temperatures were predicted for a wide range of conditions, even for some cases (low flow / low inlet quality) with channel depths as small as 0.5 mm. C_3F_8 was also found to have relatively low pressure drops and wall temperatures for a 0.5 mm channel, although wall temperature variations were relatively large along the channel length. For larger channel depths, heat transfer performance was improved for those cases with higher inlet qualities. R124 performed well for larger channel depths for a wide range of flow / inlet quality conditions. Further investigation of two-phase cooling for this application should include consideration of material compatibility, radiation hardness, ladder structural (pressure) limitations, system design concerns, and actual mockup testing.

Applicable Codes: N/A

INTRODUCTION

Two-phase cooling is being considered for the BTeV pixel detector ladders. The beryllium cooling channel under consideration is shown in Figure 1, which was taken from Reference 1. The depth of the channel has not been established but will be between 0.5 and 2.0 mm [2]. A considerable amount of heat is to be removed from the pixel modules mounted on either side of this ladder. This heat is applied only in the region with the serpentine channel. In order to minimize the effect of radiation damage on silicon operability, it is desired to maintain module temperatures on the order of -10°C.

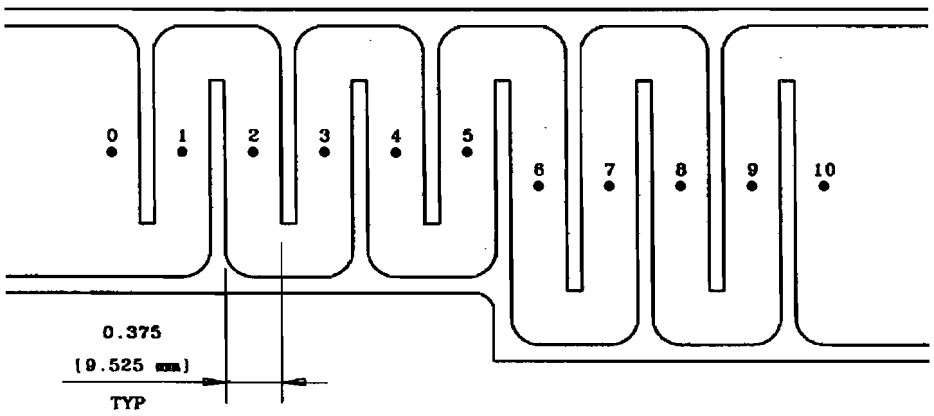

Figure 1 – Cooling Channel Configuration

The purpose of this report is to investigate performance of several refrigerants to help evaluate the feasibility of utilizing two-phase coolants with the present ladder design. Table 1 lists the potential coolants considered.

Table 1 – Refrigerants Under Consideration

Refrigerant:	**R124**	**R134a**	**Perfluoropropane (or Octofluoropropane)**
Chemical Form:	$CH\,Cl\,F\,CF_3$	$CH_2\,F\,CF_3$	C_3F_8
Radiation Length for Liquid at -20°C (cm):	19.5	26.0	22.4
P_{SAT} at -20°C (psia):	10.4	19.2	29.5
P_{SAT} at +20°C (psia):	47.4	82.9	110.0
Flammable?:	No	No	No
Atmospheric Friendliness:	"Low ozone-depletion potential"	"Ozone-depletion potential of zero"	"Zero ozone depletion potential" but "high global warming potential"
MSDS Copy Available at:	http://www.dupont.com/msds/40_37_2200fr.html	http://www.dupont.com/msds/40_37_2187fr.html	http://products.mmm.com/US/MSDS/msdsSearch.jhtml (enter "3218" under "Trade name")
Comments:	Used in industrial systems	Used in industrial and automotive AC systems	To be used in the ATLAS pixel detector at CERN

It should be noted that only the serpentine pressure drop and heat transfer characteristics of the candidate refrigerants are considered here. *Other important factors, such as chemical compatibility, coolant radiation hardness, and system design, are considered to be outside the scope of this report.*

ANALYSIS

Calculations were performed to investigate the performance of the different coolants. Fluid properties were obtained from REFPROP [3] (with the exception of C_3F_8 [4]). The iterative fluid / thermal solution techniques described below was solved with the EES code [5]. The following assumptions are made regarding the system:

a. Total heat load = 60 W (0.5 W/cm^2 on each mounting side of the detector) [2, 6]

b. Saturated refrigerant is assumed to enter the serpentine section of the ladder at -20°C. Due to the nature of two-phase cooling, this temperature could be adjusted by a change in the regulated system pressure.

c. Several cases are run, varying the inlet quality and the inlet-to-outlet quality rise to investigate performance over a wide range of conditions.

d. Channel depths of 0.5, 1.0, and 2.0 mm were investigated.

e. The serpentine section of the cooling channel was modeled as 10 separate elements. Characteristics of each of these sections are shown in Table 2.

Table 2 – Model Breakdown of Ladder Channel

Element Between Nodes Shown in Figure 1	Actual Length (mm)	Effective Length (mm)	Elevation Change (mm)	Percentage of Total Heat Load (%)
0 – 1	23.34	$L_{actual} + L_{entrance}$	12.0	5.0
1 – 2	46.68	$L_{actual} + L_{180°}$	12.0	10.0
2 – 3	46.68	$L_{actual} + L_{180°}$	12.0	10.0
3 – 4	46.68	$L_{actual} + L_{180°}$	12.0	10.0
4 – 5	46.68	$L_{actual} + L_{180°}$	12.0	10.0
5 – 6	52.68	$L_{actual} + L_{180°}$	12.0	11.2
6 – 7	58.68	$L_{actual} + L_{180°}$	12.0	12.4
7 – 8	58.68	$L_{actual} + L_{180°}$	12.0	12.4
8 – 9	58.68	$L_{actual} + L_{180°}$	12.0	12.4
9 – 10	29.34	$L_{actual} + L_{exit}$	12.0	6.2
$L_{entrance} / D_h = 20$ $L_{180°} / D_h = 60$ $L_{exit} / D_h = 20$				

Given the heat load and specified inlet and outlet qualities, the mass flowrate can be determined from an energy balance:

$$\dot{Q} = \dot{m} \cdot \left[\left(h_f + x \cdot h_{fg} \right)_{out} - \left(h_f + x \cdot h_{fg} \right)_{in} \right] \tag{1}$$

where $\dot{Q}$ = ladder total heat generation rate (W)
$\dot{m}$ = mass flowrate (kg/s)
h = enthalpy (W/kg)
f, g, or fg = subscript denotes liquid, gas, or vaporization values of a particular property
x = flowing quality = $\dot{m}_{gas} / \dot{m}_{total}$

However, for saturated coolant conditions, liquid and gas enthalpies are a function of the local bulk coolant temperature, which is in turn a function of the local pressure. Since pressure decreases in the coolant as it travels along the tube, a significant variation in physical properties can occur. Therefore, the flowrate and pressure drop relationships must be solved simultaneously.

Estimation of pressure drop in two-phase applications is not a simple calculation. Research in the field is largely geared towards a limited selection of fluids and often results in empirical correlations that are rather specific in nature. Therefore, only the simplest of pressure drop correlations, the "Homogeneous Flow Model," is utilized here [7]. This model assumes no 'slip' in the coolant – liquid and gas phases are assumed to travel at the same velocities. Previous work by the author on high-pressure water systems with vertical flow compared several models to experimental data and found the homogeneous correlation to perform quite well for those conditions [8]. It is assumed that this model will yield reasonably accurate results here such that a basic evaluation of system trends can be performed. By making the following assumptions, the homogenous flow correlation reduces to the form shown in Equation 2. Note that pressure drops are calculated for small elements along the tube length, thus the subscript 'i'. In addition to helping provide a better illustration of system performance along the detector length, the small ΔP_i values for each element, and the subsequent reevaluation of physical properties, help satisfy the assumption 'e' constraint. It should be noted that values assumed in determining ΔP_i were simply based on the pressure found in the previous element, 'i - 1', thus simplifying the solution process.

Simplifying assumptions made to the generalized homogeneous flow model:

a. Steady state
b. Constant heat flux along the channel length
c. Constant cross-sectional flow area
d. Constant mass flowrate
e. Small static pressure changes

$$P_i = P_{i-1} - \frac{\dfrac{f_{TP}\cdot p_{chan}\cdot G^2}{2\cdot A\cdot \overline{\rho}} + \overline{\rho}\cdot g\cdot \dfrac{dE}{dz} + G\cdot \upsilon_{fg}\cdot \dfrac{q''\cdot p_{chan}}{A\cdot h_{fg}}}{\dfrac{G\cdot q''\cdot p_{chan}}{A\cdot h_{fg}}\cdot \dfrac{d\upsilon_g}{dP}}\cdot \ln\left[1+\frac{\dfrac{G\cdot q''\cdot p_{chan}\cdot L}{A\cdot h_{fg}}\cdot \dfrac{d\upsilon_g}{dP}}{1+G^2\cdot x_i\cdot \dfrac{d\upsilon_g}{dP}}\right] \quad (2)$$

where P = pressure (Pa)

f_{TP} = homogeneous two-phase friction factor = $0.079\cdot(G\cdot D_h/\overline{\mu})^{-0.25}$ (2a)

G = mass flux (kg/s-m^2) = $\dot{m}/A$

D_h = hydraulic diameter of channel cross-section (m) = $4 * A / p_{chan}$ (2b)

A = channel cross-section area (m^2)

p_{chan} = channel cross-sectional perimeter (m)

$\overline{\mu}$ = mean two-phase viscosity = $\overline{\rho}\cdot[x\cdot\upsilon_g\cdot\mu_g + (1-x)\cdot\upsilon_f\cdot\mu_f]$ (2c)

μ = viscosity (N-s/m^2)

$\overline{\rho}$ = effective density (kg/m^3) = $\alpha\cdot\rho_g + (1-\alpha)\cdot\rho_f$ (2d)

α = void fraction = $\left[1+\left(\dfrac{1-x}{x}\right)\cdot\left(\dfrac{\rho_g}{\rho_f}\right)\right]^{-1}$ (for homogeneous flow) (2e)

υ = specific volume (m^3/kg)

L = effective channel element length (m)

q'' = effective heat flux, recalling that this value must be modified to account for differences between real and effective channel length (W/m^2)

g = acceleration due to gravity (m/s^2)

dE/dz = correction to account for differences between effective channel length and real elevation changes

Once the flowrate and pressure relations are solved, the wall heat transfer can be addressed. The equation governing the convective heat removal is shown in Equation 3.

$$q'' = \bar{h}_{TP} \cdot \left(T_{wall} - T_{bulk}\right) \tag{3}$$

where $\bar{h}_{TP}$ = mean heat transfer coefficient (W/m^2-K)
T_{wall} = mean local wall temperature (°C)
T_{bulk} = mean local coolant temperature (°C)

Determination of convection coefficient values is again an area of engineering limited to empirical relationships based on available test data. This study utilizes the work performed by Chen [7], whose correlation was developed based on experimental data on water and various organic fluids. Again, it is assumed that this model will yield reasonably accurate results such that a basic evaluation of system trends can be performed. Chen's correlation is expressed in Equation 4. Note that T_{wall} appears in Equations 3, 4c, and 4d, requiring an iterative solution technique.

$$\bar{h}_{TP} = 0.023 \cdot \left[\frac{G \cdot (1-x) \cdot D_h}{\mu_f}\right]^{0.8} \cdot \left[\frac{\mu \cdot c_p}{k}\right]_f^{0.4} \cdot \left(\frac{k_f}{D_h}\right) \cdot F_{Chen} + 0.00122 \cdot \left[\frac{k_f^{0.79} \cdot c_{pf}^{0.45} \cdot \rho_f^{0.49}}{\sigma^{0.5} \cdot \mu_f^{0.29} \cdot h_{fg}^{0.24} \cdot \rho_g^{0.24}}\right] \cdot \Delta T_{sat}^{0.24} \cdot \Delta P_{sat}^{0.75} \cdot S_{chen} \tag{4}$$

where c_p = specific heat (J/kg-K)
k = thermal conductivity (W/m-K)
F_{Chen} = maximum of [1.0] and $[2.35 \cdot (X_{tt}^{-1} + 0.213)^{0.736}]$ [9] (4a)

$$X_{tt} = \left(\frac{1-x}{x}\right)^{0.9} \cdot \left(\frac{\rho_g}{\rho_f}\right)^{0.5} \cdot \left(\frac{\mu_f}{\mu_g}\right)^{0.1} \tag{4b}$$

ρ = density (kg/m^3)
σ = surface tension (N/m)
$\Delta T_{sat} = T_{wall} - T_{bulk}$ (4c)
$\Delta P_{sat} = P_{sat}(T_{wall}) - P_{sat}(T_{bulk})$ (4d)
$S_{Chen} = (1 + 0.12 \cdot R^{1.14})^{-1}$ for $R < 32.5$ [9] (4e)
$= \text{maximum of } [1.0] \text{ and } [(1 + 0.42 \cdot R^{0.78})^{-1}]$ for $32.5 < R < 70$ [9] (4f)

where $R = 10^{-4} \cdot \left[\frac{G \cdot (1-x) \cdot D_h}{\mu_f}\right] \cdot F_{Chen}^{1.25}$ (4g)

RESULTS

Several cases were run to investigate the effect of channel depth, inlet quality, and quality rise ("DX," which is proportional to flowrate) on the predicted pressure drop and wall temperatures. Figures 2A through 2C show the results for the **R124** refrigerant. The Figure 2A shows the estimated pressure drop through the serpentine section. No results were available for some cases. Cases with combinations of a small channel depth and a high flowrate (small DX) yield such large pressure drops that saturation temperature falls excessively low (the program terminates the case if T_{SAT} falls below -40°C). The results show that cases with larger channel depths (most 2 mm and some 1 mm cases) and lower flowrates can be found to yield pressure drops of only a few psi. Pressure drop also increases with increasing inlet quality due to higher coolant velocities.

Figure 2B shows the R124 calculated wall temperature near the serpentine inlet, which is the warmest wall temperature in the channel. Cases that acceptably converged were found to have maximum wall temperatures within about 5°C of the inlet T_{SAT} value. Figure 2C indicates the level of temperature uniformity along the serpentine path. This plot shows the difference in temperature between the warmest wall temperature (at the inlet) and the coldest wall temperature (at the outlet). The outlet is colder than the inlet since P_{SAT} decreases along the serpentine length, thus reducing T_{SAT}. The wall temperature, being influenced by both the local coolant temperature and the heat transfer coefficient, decreases along the channel length. The Figure indicates that the cases that

acceptably converged were found to have wall temperature variations of less than 9°C for a 1 mm channel depth and less than 4°C for a 2 mm depth. Note that the high conductivity of Beryllium might act to help spread heat more uniformly within the channel structure, leading to better sensor temperature uniformity. However, consideration of this effect is outside the scope of this investigation.

The next set of plots illustrates the results for **R134a**. The serpentine pressure drops are shown in Figure 3A. Again, cases with combinations of a small channel depth and a high flowrate (small DX) yield such large pressure drops that saturation temperature falls excessively low and the calculations for that case are terminated. The results show that cases with larger channel depths and lower flowrates (all 2 mm cases and most 1 mm cases) can be found to yield pressure drops of only a few psi. Some 0.5 mm channel depth cases with low flow and low inlet quality were also found to have relatively low pressure drops.

The maximum wall temperatures with R134a are found in Figure 3B. Cases that acceptably converged were found to have maximum wall temperatures within about 4°C of the inlet T_{SAT} value. Figure 3C shows the level of temperature uniformity along the serpentine path and indicates that the cases that acceptably converged were found to have wall temperature variations of only a few degrees for the 1 mm and 2 mm channel depths. Due to the higher pressure drops, temperature variations for 0.5 mm cases were higher.

The next set of plots illustrates the results for **C_3F_8**. The serpentine pressure drops are shown in Figure 4A. Again, cases with combinations of a small channel depth and a high flowrate (small DX) yield such large pressure drops that saturation temperature falls excessively low and the calculations for that case are terminated. The results show that cases with larger channel depths and lower flowrates (almost all 2 mm cases and most 1 mm cases) can be found to yield pressure drops of only a few psi. Some 0.5 mm channel depth cases with low flow and low inlet quality were also found to have relatively low pressure drops.

The maximum wall temperatures with C_3F_8 are found in Figure 4B. Many cases were found to have temperatures considerably warmer than those shown for the previous two coolants, especially for lower inlet qualities. For cases with higher inlet qualities, performance in comparable. Figure 4C shows the level of temperature uniformity along the serpentine path and indicates that the cases that acceptably converged were found to have wall temperature variations of only a few degrees for most of the 1 mm and 2 mm channel depth cases at higher inlet qualities. At lower inlet qualities, temperature variations were found to be significantly larger. Due to the higher pressure drops, temperature variations for 0.5 mm cases were also much higher.

CONCLUSIONS

The use of two-phase cooling for the BTeV pixel ladders appears to be feasible with the serpentine channel geometry considered here. Of the three refrigerants investigated, the R134a had the best pressure drop and heat transfer performance. Small pressure drops and low, relatively uniform wall temperatures were predicted for a wide range of conditions, even for some cases (low flow / low inlet quality) with channel depths as small as 0.5 mm. C_3F_8 was also found to have relatively low pressure drops and wall temperatures for a 0.5 mm channel, although wall temperature varied by about 9°C along the channel length. For larger channel depths, heat transfer performance was improved for those cases with higher inlet qualities. R124 performed well for larger channel depths for a wide range of flow / inlet quality conditions.

Any further consideration of two-phase cooling for this application should take into account the following factors:

1. Testing – Since two-phase performance is difficult to accurately predict, it is recommended that the system be mocked up and tested to confirm that the performance is acceptable.
2. Structural Considerations – The design of the ladder structure should be understood since internal pressure limits may restrict refrigerant use due to saturation pressure / temperature characteristics.

3. Radiation Hardness – A small portion of the overall refrigerant volume would continually be passing through a high-radiation environment. Sample testing of candidate refrigerants should be performed before and after irradiation to verify chemical stability. Note that C_3F_8 has been selected for use in the ATLAS pixel detector at CERN.
4. Chemical Compatibility – The materials to be used in the detector should be evaluated for use with the coolant.
5. System Design – A basic system design should be conceptualized to provide the desired flowing conditions (i.e.; control of flowrate, inlet quality, and pressure). Such a system will likely require the ability to reliably vent the refrigerant volume in the ladders in an emergency to prevent the ladders from having to withstand the full room-temperature saturation pressure.

REFERENCES

1. FNAL drawing 8918.120-MD-407006 (preliminary version as of 15 May 2001).
2. Discussion with C.M. Lei (cmlei@fnal.gov) on 25 May 2001.
3. Computer code, "REFPROP, NIST Standard Reference Database 23 Version 6.01."
4. Email from Vaclav Vacek (vaclav.vacek@cern.ch) on 21 Feb 2001.
5. Computer code, "Engineering Equation Solver (EES) Version 4.761."
6. Discussion with Rich Schmitt (rlschmitt@fnal.gov) on 14 May 2001.
7. John G. Collier and John R. Thome, "Convective Boiling and Condensation, 3rd ed.," (Oxford: Clarendon Press, 1994).
8. Greg Derylo et. al., "Two Phase Pressure Drop Calculations Using Various Models," Penn State Univ. ME 515 Design Project, March 1995.
9. Information provided to the author in 1995 by Larry Hochreiter of Westinghouse (now in the Penn State Nuclear Eng. Dept.) on the computer codes COBRA-TF and TRAC-PF1, which were developed under sponsorship by the U.S. Nuclear Regulatory Commission.

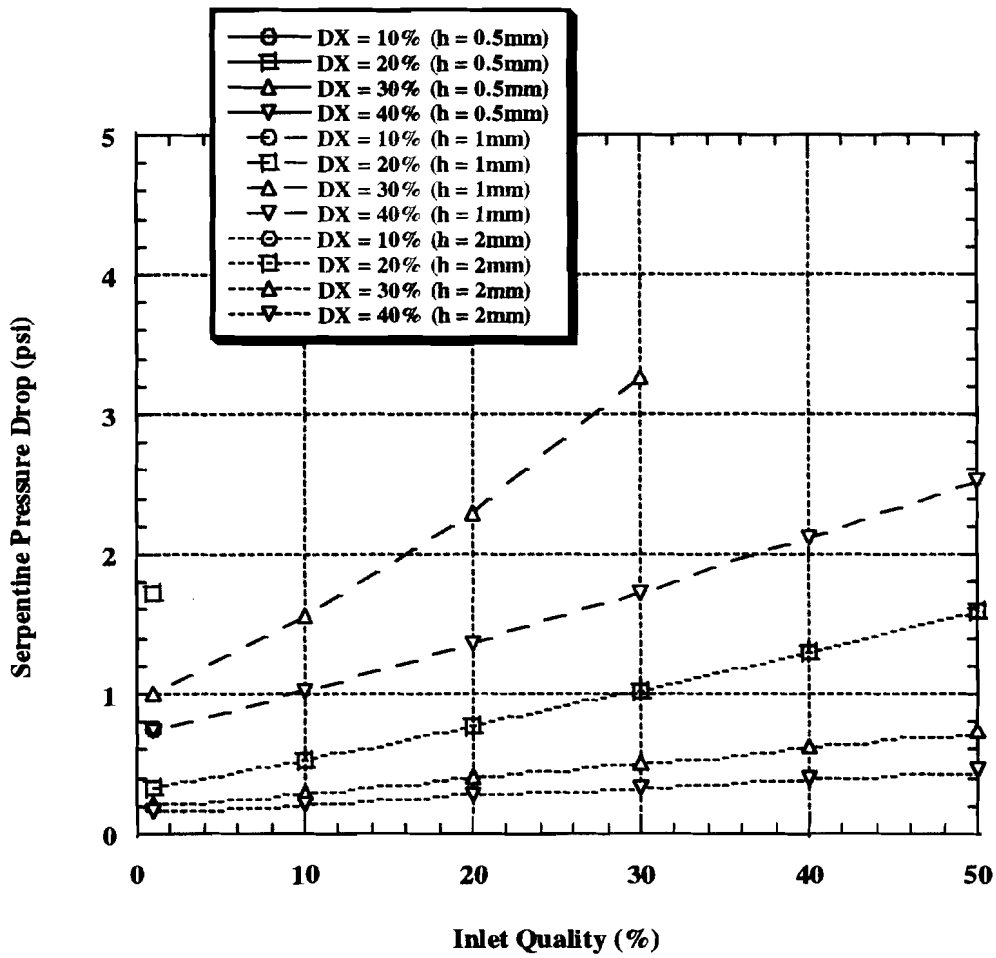

Figure 2A – Pressure Drop vs. Inlet and Differential Quality for R124

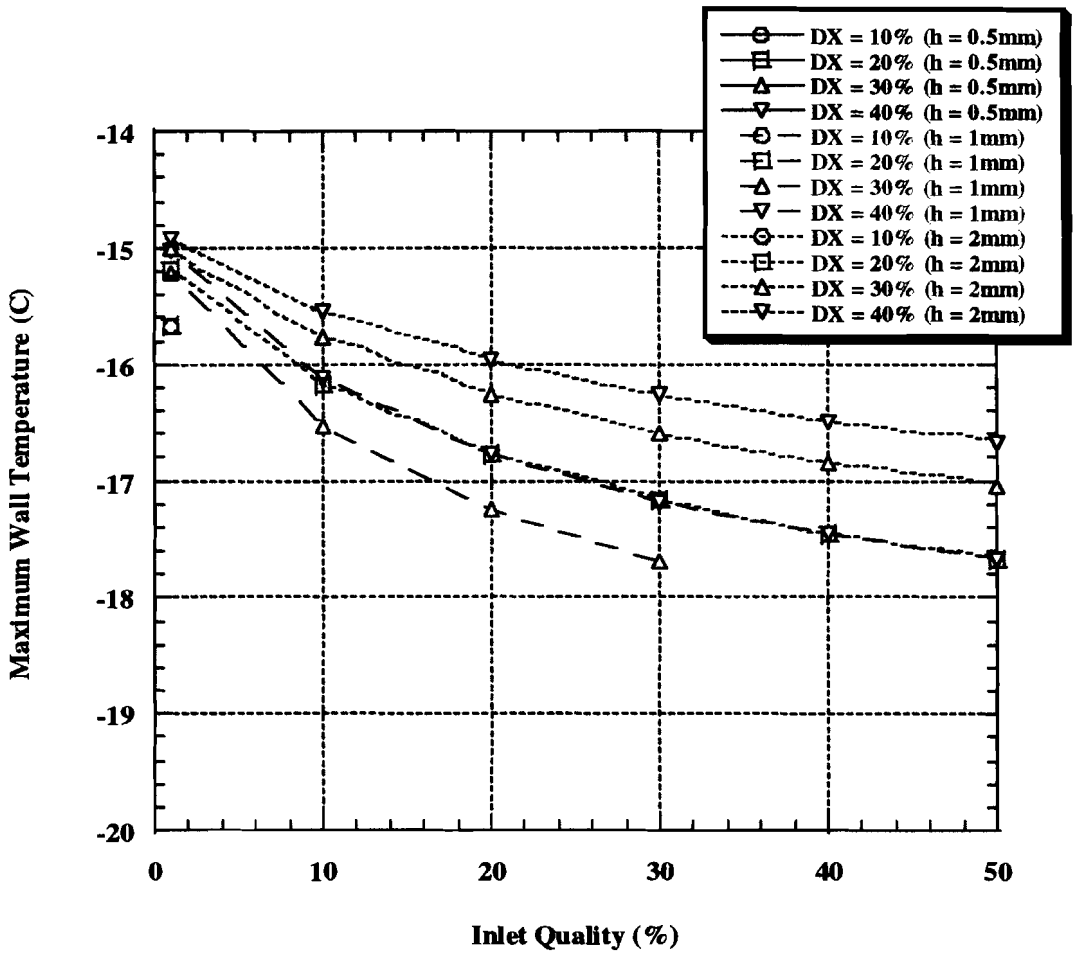

Figure 2B – Maximum Wall Temperature (located at serpentine inlet) vs. Inlet and Differential Quality for R124

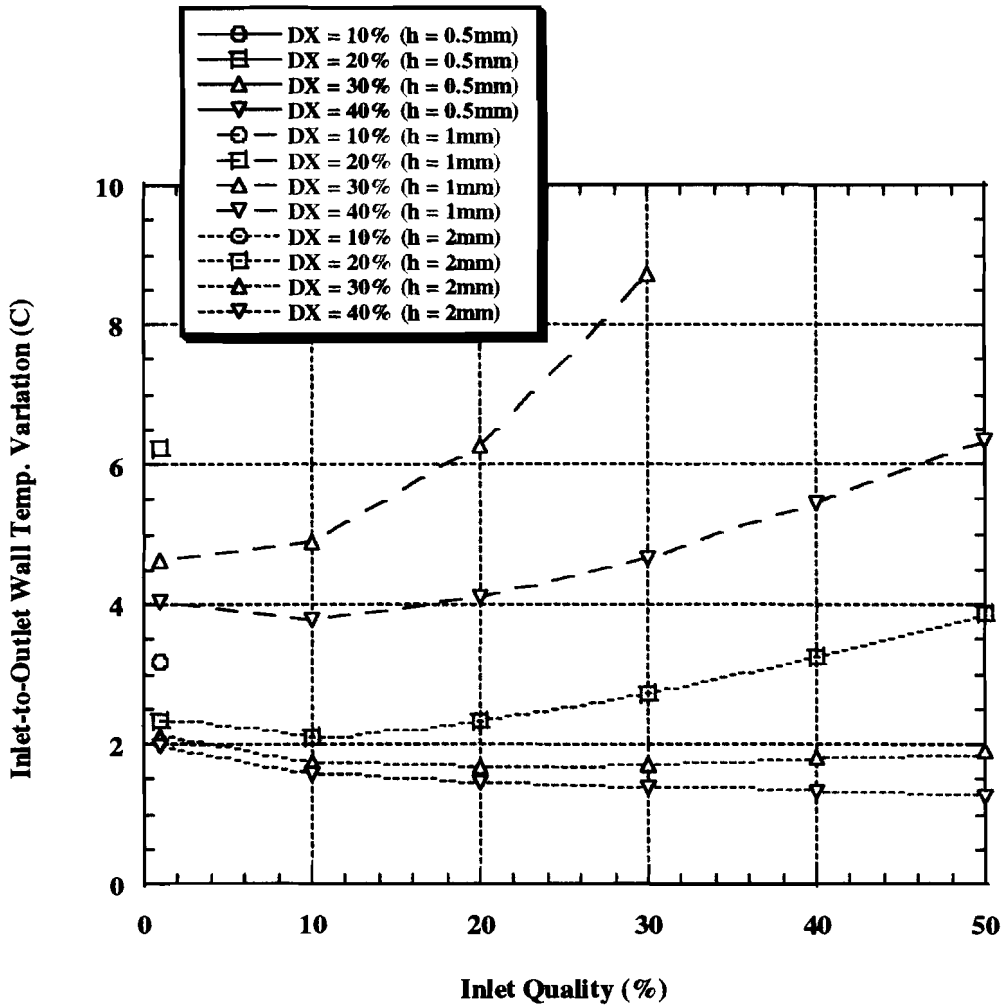

Figure 2C – Inlet-to-Outlet Wall Temperature Variation vs. Inlet and Differential Quality for R124

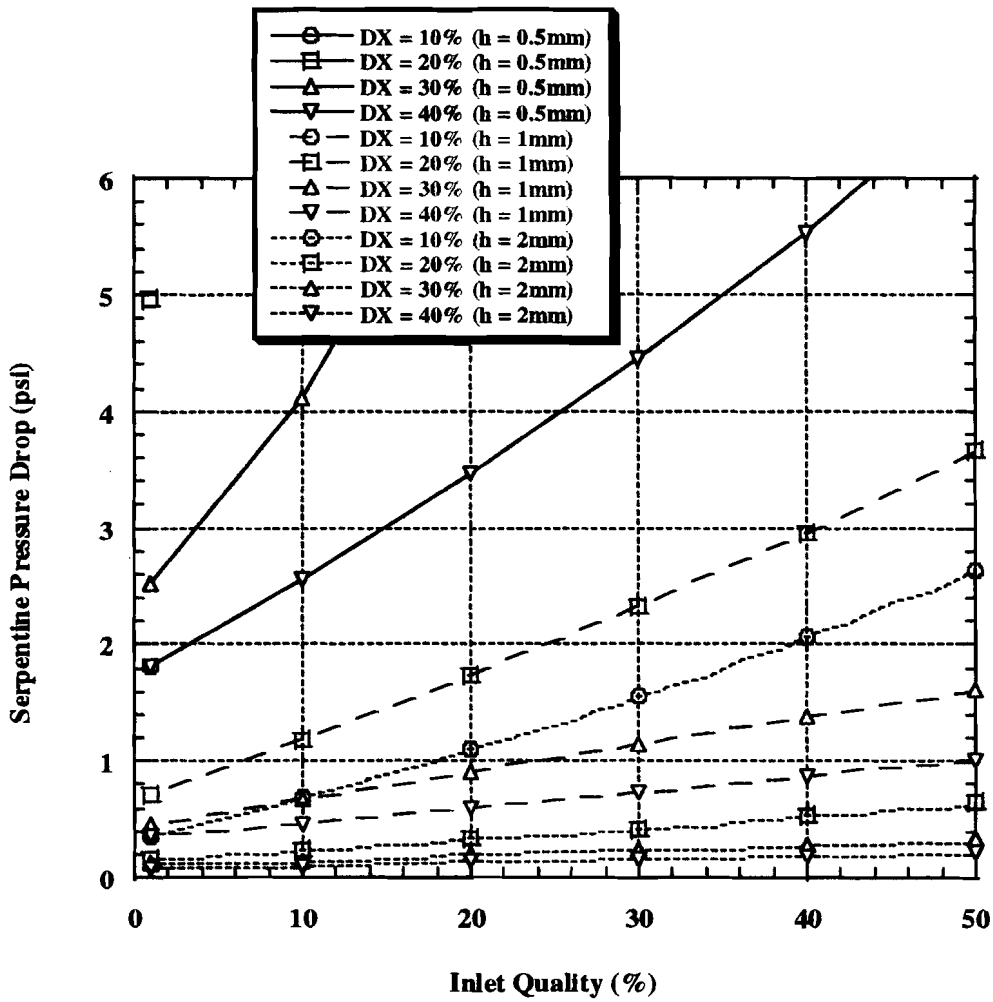

Figure 3A – Pressure Drop vs. Inlet and Differential Quality for R134a

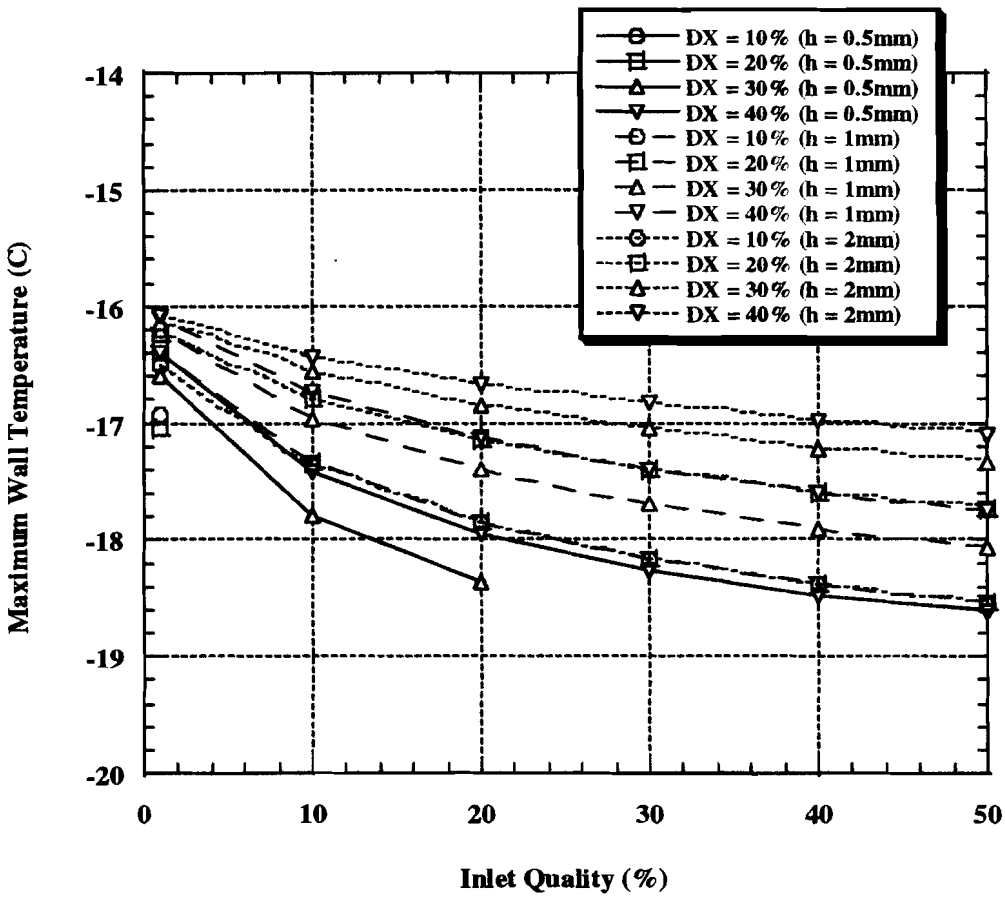

Figure 3B – Maximum Wall Temperature (located at serpentine inlet) vs. Inlet and Differential Quality for R134a

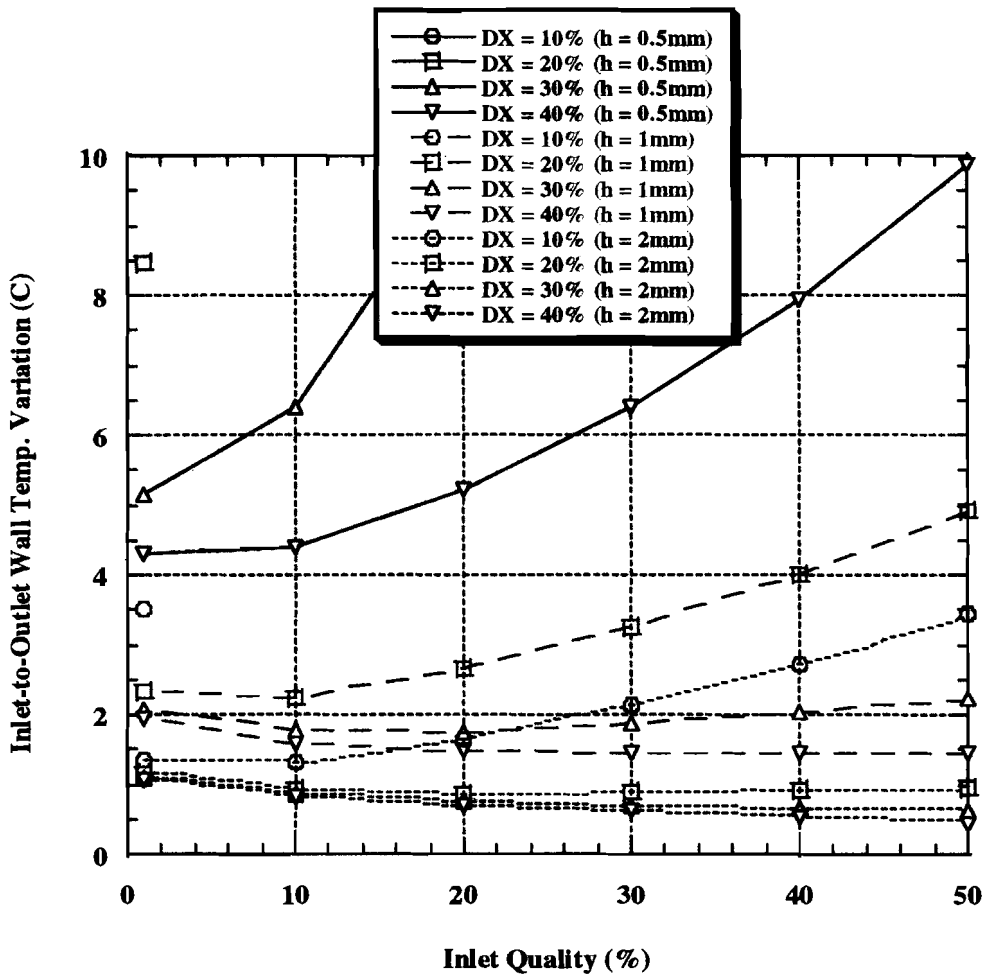

Figure 3C – Inlet-to-Outlet Wall Temperature Variation vs. Inlet and Differential Quality for R134a

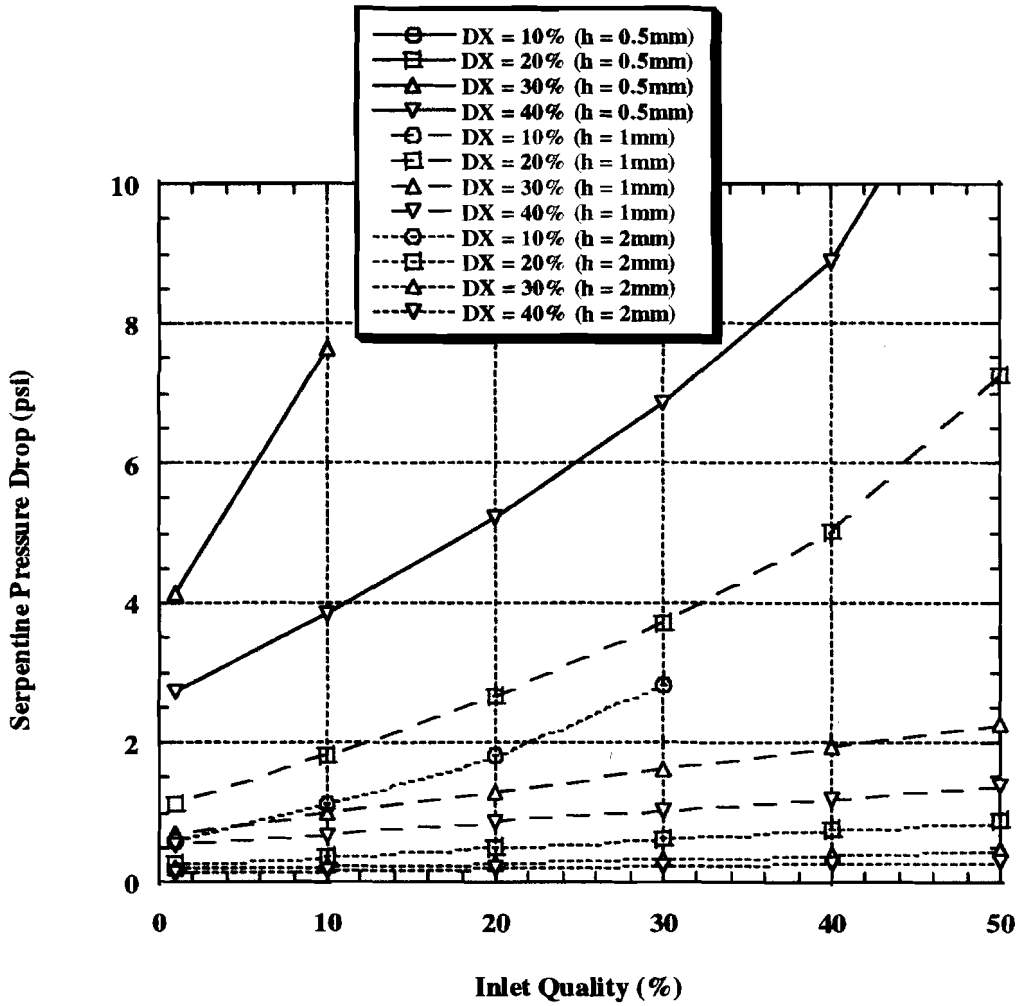

Figure 4A – Pressure Drop vs. Inlet and Differential Quality for C_3F_8

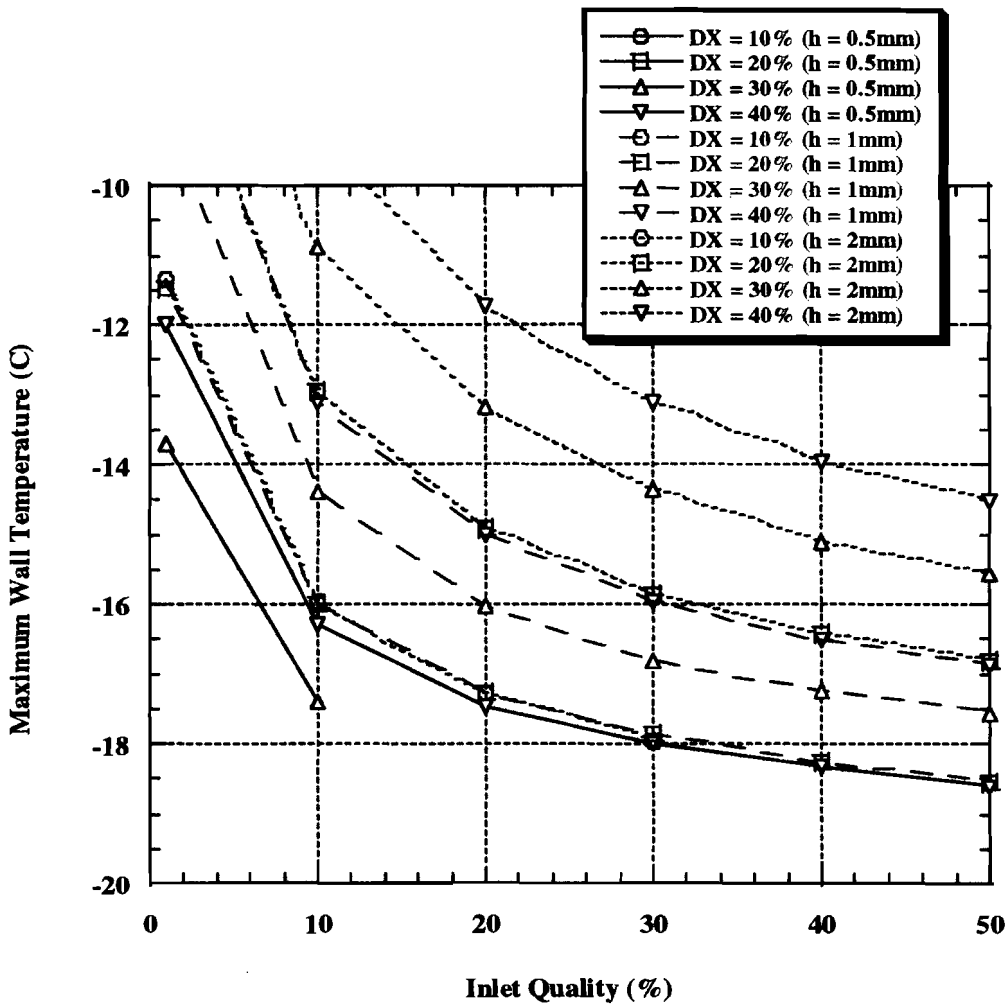

Figure 4B – Maximum Wall Temperature (located at serpentine inlet) vs. Inlet and Differential Quality for C_3F_8

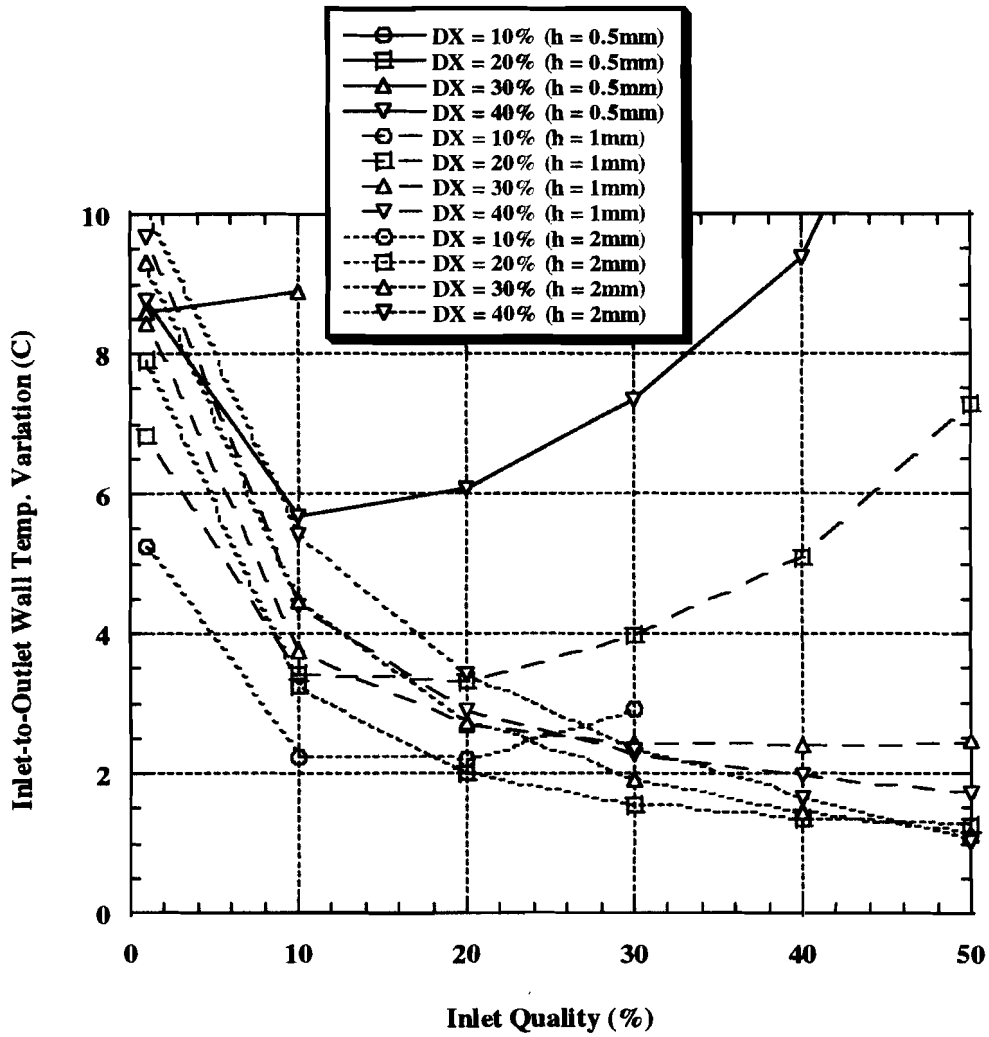

Figure 4C – Inlet-to-Outlet Wall Temperature Variation vs. Inlet and Differential Quality for C_3F_8